Cellular Microbiology (2016) **18**(6), 784–791
doi:10.1111/cmi.12559
First published online 27 January 2016

Breaking Report

Phosphorylation of influenza A virus NS1 protein at threonine 49 suppresses its interferon antagonistic activity

Omer Abid Kathum,[1,†] Tobias Schräder,[1,†] Darisuren Anhlan,[1,†] Carolin Nordhoff,[1] Swantje Liedmann,[1] Amit Pande,[2,3] Alexander Mellmann,[4] Christina Ehrhardt,[1] Viktor Wixler[1] and Stephan Ludwig[1*]

[1] *Institute of Molecular Virology (IMV), Centre for Molecular Biology of Inflammation (ZMBE), Westfaelische Wilhelms-University Muenster, Muenster, Germany.*
[2] *Institute of Experimental Pathology, Centre for Molecular Biology of Inflammation (ZMBE), Westfaelische Wilhelms-University Muenster, Muenster, Germany.*
[3] *Institute of Evolutionary and Medical Genomics, Brandenburg Medical School (MHB), Neuruppin, Germany.*
[4] *Institute of Hygiene, Westfaelische Wilhelms-University Muenster, Muenster, Germany.*

Summary

Phosphorylation and dephosphorylation acts as a fundamental molecular switch that alters protein function and thereby regulates many cellular processes. The non-structural protein 1 (NS1) of influenza A virus is an important factor regulating virulence by counteracting cellular immune responses against viral infection. NS1 was shown to be phosphorylated at several sites; however, so far, no function has been conclusively assigned to these post-translational events yet. Here, we show that the newly identified phospho-site threonine 49 of NS1 is differentially phosphorylated in the viral replication cycle. Phosphorylation impairs binding of NS1 to double-stranded RNA and TRIM25 as well as complex formation with RIG-I, thereby switching off its interferon antagonistic activity. Because phosphorylation was shown to occur at later stages of infection, we hypothesize that at this stage other functions of the multifunctional NS1 beyond its interferon-antagonistic activity are needed.

Received 6 October, 2015; revised 30 October, 2015; accepted 11 November, 2015. *For correspondence. E-mail ludwigs@uni-muenster.de; Tel. +49 251 83 57791; Fax +49 251 83 57793.
†These authors contributed equally

Introduction

Influenza A virus (IAV) non-structural protein 1 (NS1) is a highly expressed multifunctional protein playing important roles in viral replication (Hale *et al.*, 2008). It is composed of an N-terminal RNA binding domain (RBD, residues 1–73) and a C-terminal effector domain (ED, residues 74–230) (Qian *et al.*, 1995; Hale *et al.*, 2008). While the ED interacts with various host cell proteins, the RBD is also able to bind different RNA species, including viral RNA (vRNA) and double-stranded RNA (dsRNA) (Hatada and Fukuda, 1992; Qiu and Krug, 1994; Hatada *et al.*, 1997; Marc, 2014). The most important function of NS1 is to antagonize host immune responses, and accordingly, deletion of NS1 results in high attenuation of IAVs in interferon (IFN)-competent systems (García-Sastre *et al.*, 1998; García-Sastre, 2011; Marc, 2014; Krug, 2015). NS1 prevents vRNA-mediated activation of IFN-inducing pathways by sequestering vRNA from its sensor RIG-I, but also by inhibition of RIG-I signalling via interaction with RIG-I or its upstream activators TRIM25 or Riplet (Mibayashi *et al.*, 2007; Opitz *et al.*, 2007; Gack *et al.*, 2009; Rajsbaum *et al.*, 2012). Phosphorylation commonly regulates distinct activities of multifunctional proteins and also for NS1, numerous phosphorylation sites have been described (Hale *et al.*, 2009; Hsiang *et al.*, 2012; Hutchinson *et al.*, 2012). However, so far, there is only scarce information on how phosphorylation may control NS1 function.

Results and discussion

To elucidate differentially phosphorylated residues of NS1 during the IAV replication cycle, SILAC-labelled A549 human lung epithelial cells were infected with influenza virus strain A/PR/8/34 (PR8; H1N1) for different times. Mass spectrometry analysis revealed three phosphorylation sites of NS1 at positions S48, T49 and T215.

Interestingly, all three residues were identified as being phosphorylated only at late stages of viral infection presuming a functional switch of NS1 at that time (Fig. 1A, left). Noteworthy increasing phosphorylation did not simply correspond to increased NS1 expression in infected cells, as expression of NS1 was readily detectable 4 h p.i., whereas virtually no phosphorylation was detectable at that time (Fig. 1A, right). Phosphorylation of T49 as well as T215 was independently confirmed by immunoprecipitation of NS1 from infected A549 cells followed by mass spectrometry analysis (Data not shown). While phosphorylation of S48 and T215 had been reported before (Hale *et al*., 2009; Hsiang *et al*., 2012), T49 represents a new target site for phosphorylation in PR8 NS1. T215 lies in the ED, whereas both S48 and T49 are located in the RBD (Cheng *et al*., 2009; Hsiang *et al*., 2012). Crystal structure analysis of the NS1 RBD domain showed that T49 but not S48 belongs to key residues in dsRNA recognition and directly contributes to the dsRNA binding by forming hydrogen bonds (Cheng *et al*., 2009). Interestingly, in contrast to S48 and T215, T49 represents an evolutionary highly conserved residue (99.8 %) among avian, human and swine IAV isolates. Thus, we focused on the functional analysis of phosphorylation of the newly identified site at T49 compared to T215, which was previously shown to have a minor impact on viral replication (Hsiang *et al*., 2012). By reverse genetics we generated recombinant PR8 virus mutants in which T49 or T215 of NS1 were exchanged either for non-phosphorylatable (T49A, T215L) or for negatively charged residues mimicking constitutive phosphorylation (T49E, T215D) (Hoffmann *et al*., 2000). To analyse viral replication, MDCKII cells were infected with wt (PR8/NS1-T49 or PR8/NS1-T215) or mutated PR8 viruses (PR8/NS1-T49A, PR8/NS1-T49E, PR8/NS1-T215L or PR8/NS1-T215D). While T215L or T215D mutations, as suggested from earlier studies (Hsiang *et al*., 2012), did not significantly alter viral progeny, exchange of T49 for glutamic acid but not for alanine resulted in significantly decreased viral titers (Fig. 1B and C), strongly indicating that phosphorylation of NS1 at T49 negatively affects viral replication. This was further confirmed by Western blot analysis of viral PB1, NP and NS1 protein expression in infected MDCKII cells (Fig. 1D and E). Significantly attenuated viral replication was also evident in A549 lung epithelial cells infected with the PR8/NS1-T49E virus, thus fully confirming the results from MDCKII cells (Supporting Information Fig. S1 A and B).

As inhibition of type I IFN induction is one of the major tasks of the NS1 protein, we wondered whether the attenuated replication by phosphorylation-mimicry at T49 in the PR8/NS1-T49E virus might be due to increased induction of IFNβ. Therefore, A549 cells were infected with wt or NS1-mutated viruses for different times, and the levels of IFNβ mRNA were investigated by qRT-PCR. Indeed, of all studied NS1 mutants, only the T49E

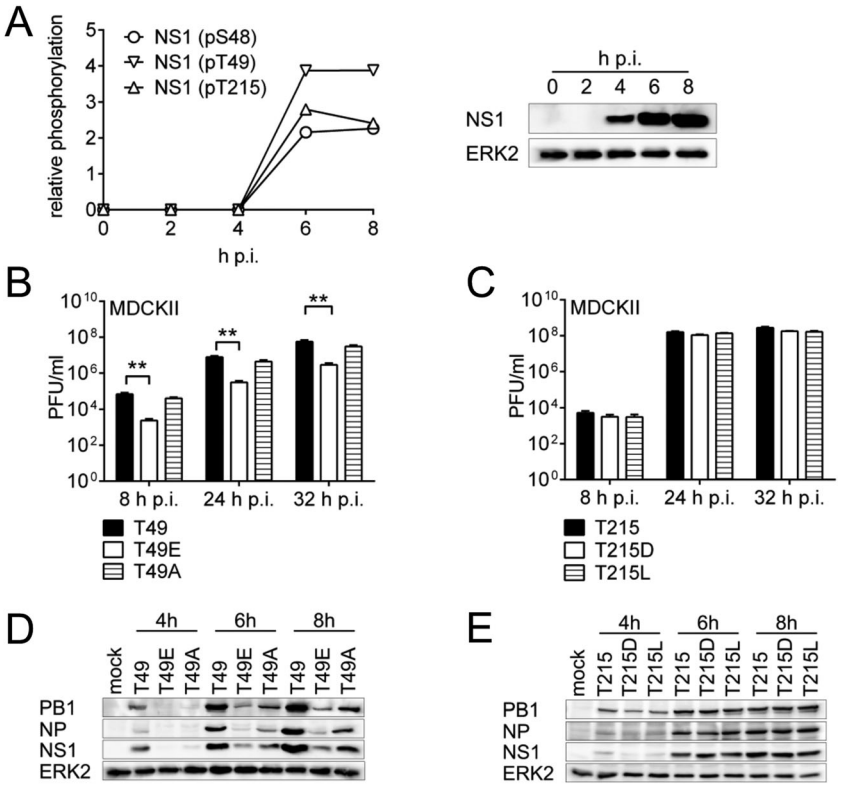

Fig. 1. Phosphorylation of NS1 at T49 but not T215 attenuates viral replication.
A. The NS1 protein is phosphorylated at several sites later in infection cycle. SILAC labelled A549 cells were infected with PR8 (MOI = 5) for the indicated times and were either subjected to a LC-MS/MS analysis as described in experimental procedures or analysed for NS1 expression by Western blotting using mouse anti-NS1 antibody for detection of NS1. ERK2 served as loading control.
B, C. Multi-cycle replication kinetics of recombinant PR8 viruses containing wt NS1 or NS1 with different mutations. MDCKII cells were infected with low multiplicity of infection (MOI = 0.01) and supernatants of infected cells were analysed for virus progeny by standard plaque assay. Data represents mean ± SD of three independently repeated experiments. One-way ANOVA followed by Dunnett's multiple comparisons test using T49 or T215 as controls was used for statistical analysis of each time point separately (**$p \leq 0.01$).
D, E. Viral protein expression in MDCKII cells infected with wt or NS1 mutated PR8 viruses (MOI = 5). Cells were lysed at the indicated time points and subjected to SDS-PAGE followed by Western blotting. Antibodies used were against viral PB1, NP and NS1 proteins. ERK2 served as loading control.

mutation conferred a strong IFN gene induction (Fig. 2A and B), indicating that this mutant is less capable of suppressing the cellular IFN response.

The IFN promoter comprises three functional transcription factor binding sites for AP-1, NF-κB and IRF-3, with IRF-3 being the most important site for virus-specific induction of gene expression downstream of RIG-I. To reveal if IFN promoter activity was influenced by the T49E substitution in NS1, luciferase reporter gene assays with reporter gene constructs harbouring sites for either all three domains of the promoter or for IRF-3-only were performed. We found that in cells stimulated with vRNA, NS1-T49E was less capable of inhibiting the activation of the IFNβ-induced and IRF-3-driven promoter compared with NS1 wt or NS1-T49A (Fig. 2C and D). Therefore, NS1-T49E had a severe defect in the ability to suppress the IRF-3 mediated activation of IFNβ expression. This finding strongly suggests that the induction of type I IFN might be responsible for the attenuation of the PR8/NS1-T49E virus. Indeed, this virus mutant lost its attenuation when Vero cells that are devoid of functional type I IFN genes were infected (Fig. 2E). This finding could also be confirmed *in vivo* in *Ifnar1*$^{-/-}$ mice deficient for the type I interferon receptor (Fig. 2F). These data strongly indicate that a negative charge at T49 of NS1 abrogates its IFN-suppressive function leading to an attenuated virus phenotype *in vitro* as well as *in vivo*.

The IFN antagonistic activity of NS1 involves binding and sequestration of RNA as well as direct interaction with TRIM25 and complex formation with the RNA sensor RIG-I (Mibayashi *et al.*, 2007; Hale *et al.*, 2008). Therefore, we next addressed whether the observed enhancement of IRF-3 activity and IFNβ expression by PR8/NS1-T49E was due to altered binding or complex formation with RNA and/or RIG-I/TRIM25.

Indeed, the RNA binding capacity of NS1-T49E was significantly reduced, indicating that negative charging or phosphorylation of NS1 at T49 negatively affects its RNA

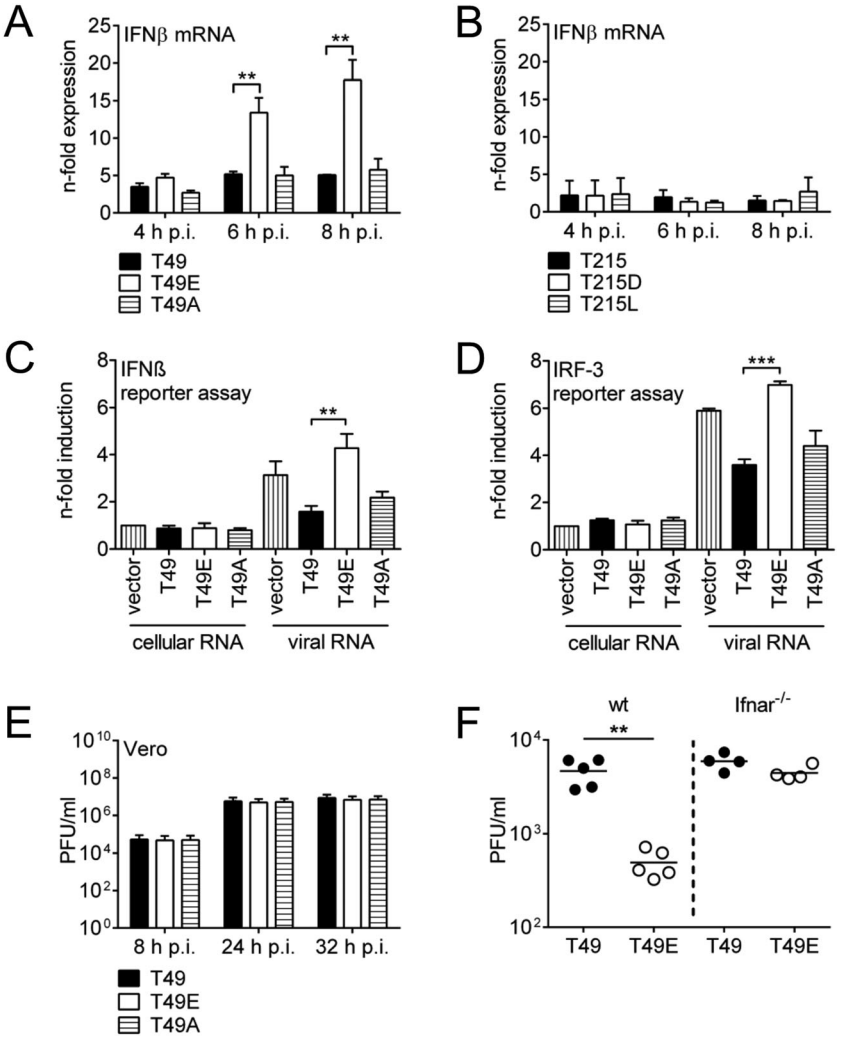

Fig. 2. The T49E substitution affects interferon β (IFNβ) antagonistic properties of NS1.
A, B. IFNβ mRNA expression in A549 cells infected with recombinant PR8 viruses containing wt NS1 or NS1 with different mutations (MOI = 5) was measured by qRT-PCR. Values represent *n*-fold expression of mock-infected cells and are displayed as mean ± SD of three independently repeated experiments. One-way ANOVA followed by Dunnett's multiple comparisons test using T49 or T215 as controls was used for statistical analysis of each time point separately (**$p \leq 0.01$).
C, D. Phosphorylation of NS1 T49 suppresses IFNβ promoter activity. A549 cells were transfected with pcDNA3 plasmids containing different NS1 genes and with luciferase reporter gene plasmids harbouring the IFN promotor or the IRF-3 domain only. After 24 h, cells were stimulated with vRNA or cellular RNA and luciferase activity in cell lysates was measured after 6 h. Results represent means ± SD of three independently repeated experiments. Luciferase activity of empty vector transfected, cellular RNA stimulated cells was taken as unity. Statistical significance of vRNA stimulated cells was analysed by one-way ANOVA followed by Dunnett's multiple comparisons test using T49 as control (**$p \leq 0.01$, ***$p \leq 0.001$).
E. Multi-cycle replication kinetics of recombinant PR8 viruses with wt NS1 or NS1 with different mutations in Vero cells infected at a MOI of 0.01. Results represent means ± SD of three independently repeated experiments.
F. Viral replication in lungs of C57Bl/6 and C57Bl/6 *Ifnar1*$^{-/-}$ mice. Mice were infected with 10^3 PFU of PR8/NS1-T49 or PR8/NS1-T49E and lung virus titers were determined after 3 days. PFU/ml of lung homogenate are presented. Statistical analysis was performed using the Mann-Whitney U test (**$p \leq 0.01$).

binding (Fig. 3A). In addition, based on published structure data of NS1 RBD/dsRNA (Cheng *et al*., 2009), we performed a computational calculation of RNA binding to wt and mutated NS1, which fully matched the experimental data (Fig. 3B). The effect of single residue change (T49E) on protein structure was further probed using HOPE (not shown) and DUET predication servers (Venselaar *et al*., 2010; Pires *et al*., 2014b). Figure 3C left shows that T49 (in red) sits in close proximity to dsRNA to form hydrogen bonds. In contrast, E49 (in purple), that brings in a RNA-repelling negative charge, is unable to form hydrogen bonds because of a stereo-chemically incorrect position, which also leads to further structural changes of the RBD that in turn might also influence TRIM25 or RIG-I binding or complex formation (Fig. 3C, right).

The complex formation of NS1 with RIG-I was indeed strongly reduced with the T49E mutant compared with wt NS1 or NS1-T49A, as shown by co-immunoprecipitation assays from cell lysates after transient co-expression of FLAG-tagged RIG-I and NS1 (Fig. 3D). Consistently, NS1-T49E expressed from a mutant virus in infected HEK293 cells less efficiently co-precipitated endogenous TRIM25 (Fig. 3E).

In summary, our data demonstrate for the first time that the multifunctional NS1 protein is differentially phosphorylated throughout the replication cycle and that phospho-modification at T49 acts as a molecular switch that alters

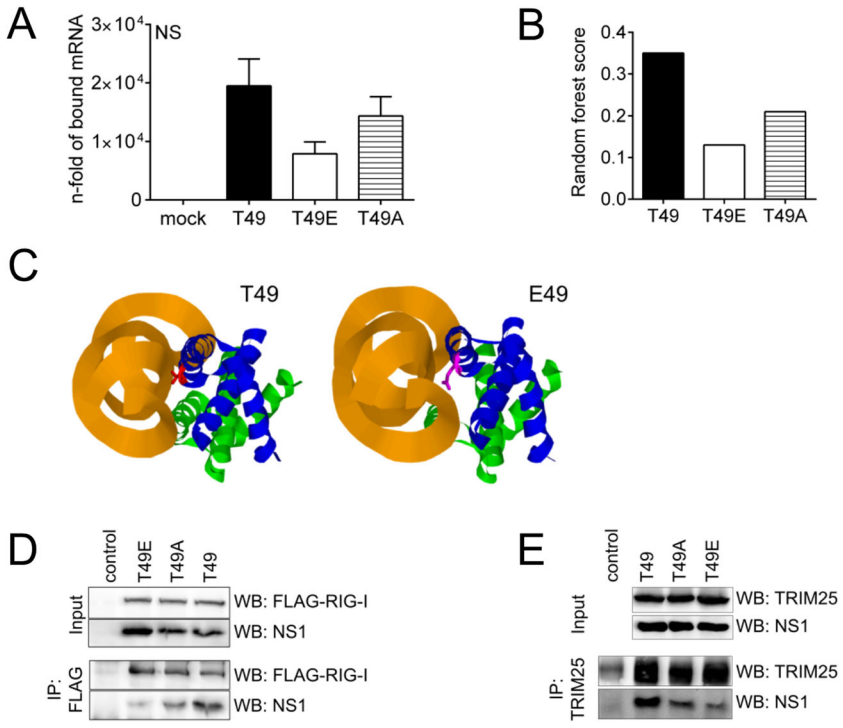

Fig. 3. Phosphorylation of NS1 T49 leads to reduced vRNA, RIG-I and TRIM25 binding as well as structural destabilization of the RBD.
A. A549 cells were transfected with pcDNA3 plasmids containing wt NS1 or NS1 with indicated mutations or were mock transfected. Cell lysates were subjected to immunoprecipitations 24 h p.i. using mouse anti-NS1 antibody. Washed beads were incubated with vRNA and RNA bound to immunocomplexes was extracted. The relative amount of viral NS1 mRNA was determined by qRT-PCR as described previously (Habjan *et al*., 2008). Data represents mean ± SD of two independently repeated experiments.
B. Comparative binding scores of RNA to RBD T49E, T49A and T49 as calculated using random forest model from the RNA–protein interaction prediction (RPISeq) tool (Muppirala *et al*., 2011). The RNA sequence was obtained from Protein Data Bank (PDB) ID 2ZKO (Cheng *et al*., 2009).
C. Structural simulation on 2ZKO structure employing DUET (Pires *et al*., 2014B) was predicted as destabilizing (−0.17 Kcal/mol) resulting in an unfavourable RNA binding ability. The figure shows the stereo-chemical effect of E49 compared with T49. The RNA helix is shown in yellow, while the two monomers of the NS1 dimer are shown in green and blue. NS1 residues T49 and E49 are shown in red and purple respectively. Molecular graphic simulation was performed using Bioblender (Andrei *et al*., 2012).
D. For analysis of NS1-RIG-I interaction, HEK293 cells transiently expressing FLAG-tagged RIG-I and the indicated NS1 proteins were subjected to crosslinking with DSP after 48 h, followed by quenching with glycine. Control cells were mock transfected. FLAG-tagged RIG-I was immunoprecipitated with anti-FLAG M2 antibody. Detection of FLAG-tagged RIG-I and co-precipitated NS1 protein was performed by Western blotting. Detection of FLAG-tagged RIG-I and NS1 in the cell lysates before immunoprecipitation served as 'input control' ensuring comparable expression levels.
E. For analysis of NS1-TRIM25 interaction HEK293 cells were infected with PR8/NS1-T49, PR8/NS1-T49A or PR8/NS1-T49E (MOI of 1, 5 or 10 respectively) or were mock infected (control).Eighteen h p.i. cells were lysed and lysates subjected to immunoprecipitation with mouse anti-TRIM25 antibody. TRIM25 and the co-precipitated NS1 were detected by Western blotting using mouse anti-TRIM25 antibody or mouse anti-NS1 antibody. Detection of TRIM25 and NS1 in the cell lysates before immunoprecipitation served as 'input control' ensuring comparable expression levels.

NS1 activity. In early stages, NS1 is unphosphorylated, allowing strong complex formation with RNA, TRIM25 as well as RIG-I, which results in efficient suppression of IFN induction. However, at later stages, NS1 gets phosphorylated at T49, leading to reduced interaction with RNA, TRIM25 and RIG-I. Although it might be argued that our experiments do not provide full evidence of effects on direct binding because of the lack of biochemical assays with purified proteins, we would still tend to conclude that, in reference to published data (Mibayashi *et al*., 2007; Hale *et al*., 2008), the reduced amounts of co-immunoprecipitated RNA, TRIM25 or RIG-I are indicative of an impaired binding that is of biological relevance. This results in decreased IFN antagonistic activity, which might be dispensable at that stage, allowing NS1 to fulfill other important functions that remain to be identified.

It is noteworthy to mention that another interpretation of the data might be that phosphorylation of NS1 at T49 represents an antiviral event induced by the cell to limit viral replication. However, given that residue 49 in IAV NS1 is highly conserved throughout evolution, this interpretation seems to be very unlikely. The virus would have easily escaped that antiviral attack by mutation of the site. Thus, the phosphorylation induced functional switch seems to be important for viral replication. This notion is further confirmed by the fact that, in addition to the T49E substitution, also the non-phosphorylatable T49A substitution negatively affected viral titers and protein expression, although to a much lesser extend. Thus, not only the negative charge at T49 in early stages is unfavourable for the virus but also the lack of phosphorylation in later stages. From the data, it also can be concluded that it is more important for replication to keep NS1 T49 in an unphosphorylated state at early time points than to add a phospho-modification at late stages. In summary, we hypothesize that phosphorylation of NS1 at T49 switches-off its IFN antagonistic activity and may direct the protein to other functions that, e.g. support release of mature viral particles. This switch seemed to be indispensable for efficient viral replication.

Experimental procedures

Cell lines, virus strains and viral infections

The human lung adenocarcinoma cells (A549), the human embryonic kidney cells (HEK293) and the African green monkey epithelial cells (Vero) were grown in Dulbecco's modified Eagle's medium (Sigma-Aldrich). The Mardin-Darby canine kidney cells (MDCKII) were grown in minimum essential medium (Sigma-Aldrich). Dulbecco's modified Eagle's medium and minimum essential medium were supplemented with 10% fetal calf serum (Merck-Millipore). Cells were cultivated at 37°C and 5% CO_2 under constantly humidified conditions.

Human influenza virus A/Puerto Rico/8/34 (PR8; H1N1) wt virus and mutants used in this study were generated by the pHW2000-based eight plasmid reverse genetics system as described elsewhere (Hoffmann *et al*., 2000). Infection of either A549 or MDCKII cells was performed at a defined multiplicity of infection (MOI) for the indicated times as described previously (Dudek *et al*., 2010).

Phosphoproteomic screening of infected cells

For the screening of influenza A virus NS1 phosphorylation, the stable isotope labelling by amino acids in cell culture (SILAC) method was used. Human A549 cells stably labelled with either 'light' lysine ($^{12}C_6$, $^{14}N_2$) and arginine ($^{12}C_6$, $^{14}N_4$), 'medium' lysine ($^{13}C_6$, $^{14}N_2$) and arginine ($^{13}C_6$, $^{14}N_2$) or 'heavy' lysine ($^{13}C_6$, $^{15}N_2$) and arginine ($^{13}C_6$, $^{15}N4$) were infected with PR8 (MOI = 5) for 0, 2, 4, 6 and 8 h. Thereby 'medium'-labelled and 'heavy'-labelled cells were infected for 2 or 6 h and 4 or 8 h, respectively, while 'light'-labelled cells were always used as non-infected controls (0 h). Lysates from cells infected for 0, 2 and 4 h were mixed equally and used as first sample, while equally mixed lysates from cells infected for 0, 6 and 8 h as second sample. After tryptic digestion samples were subjected to cation exchange chromatography and TiO_2-based phosphopeptide enrichment chromatography followed by LC-MS/MS analysis on a Proxeon Easy-nLC coupled to an LTQ-Orbitrap XL mass spectrometer. The data were then processed using Mascot and MaxQuant software (v1.2.2.9) as previously described (Macek *et al*., 2009; Carpy *et al*., 2014). Phosphorylation intensity of NS1 residues was quantified in relation to the amount of total NS1 protein expressed and 'light'-labelled cells in both lysate mixtures were used as controls.

Standard plaque titration

The number of infectious particles in the supernatant of infected cells was determined by standard plaque titration as described earlier (Dudek *et al*., 2010).

Lysis of cells and Western blotting

Viral protein expression was analysed by Western blotting. At the indicated times after infection, the cell monolayer was washed with PBS (Sigma) and cells were lysed in RIPA buffer (25 mM Tris-HCl [pH 8], 137 mM NaCl, 10 % glycerol, 0.1 % sodium dodecylsulfate, 0.5 % sodium deoxycholate, 1 % Igepal, 2 mM EDTA [pH 8]) supplemented with protease inhibitors. Lysates were cleared by centrifugation (20000 × g, 4°C, 10 min). The clear supernatant was then mixed with Laemmli sample buffer and boiled for 5 min at 95°C. Equal amounts of total protein were used for separation in sodium dodecyl sulfate-polyacrylamide gel electrophoresis (SDS-PAGE). Proteins were blotted onto nitrocellulose membranes (GE Healthcare). Incubation with the primary antibodies goat anti-PB1 (clone vK-20, Santa Cruz), mouse anti-NP (clone AA5H, AbD Serotec), mouse anti-NS1 (clone NS1-23-1, IMV Münster) or rabbit anti-ERK2 (Santa Cruz) diluted in TBST buffer (50 mM Tris-HCl [pH 7.5], 150 mM NaCl, 0.2 % Triton X-100) was performed over night at 4°C. Horseradish peroxidase labelled secondary antibodies anti-goat (Jackson

ImmunoResearch Laboratories or Santa-Cruz), anti-mouse (Jackson ImmunoResearch Laboratories or Cell Signalling) or anti-rabbit (Bio-Rad or Cell Signalling) were diluted in TBST and incubation was performed for 0.5–1 h at room temperature. Visualisation was performed by enhanced chemiluminescence reaction.

RNA isolation, cDNA synthesis and quantitative real-time polymerase chain reaction

Isolation of RNA was performed using the RNeasy Mini Kit or RNeasy Plus Mini Kit (Qiagen) according to the manufacturer's protocol. Concentration of isolated total RNA was measured by a Nanodrop ND-1000 spectrophotometer (Peqlab). Equal amounts of RNA were used to synthesize cDNA with the Revert AID H Minus Reverse Transcriptase (Thermo Fisher Scientific) and oligo (dT) primers (Eurofins MWG Operon) according to the manufacturer's protocol. The quantification of cDNA was performed by quantitative real-time polymerase chain reaction (qRT-PCR) using the Mx Pro 3005P cycler (Stratagene) and the following primers: GAPDH_fwd 5′-gcaaattccatggcaccgt-3′, GAPDH_rev 5′-gccccacttgattttggagg-3′, IFNβ_fwd 5′-tctggcacaacaggtagtaggc-3′, IFNβ_rev 5′-gagaagcacaacaggagagcaa-3′, NS1_fwd 5′-tgccttctcttccaggacat-3′, NS1_rev 5′-ccattcaagtcctccgatg-3′. The qRT-PCR reaction mix (Brilliant III SYBR Green QPCR Master Mix) was purchased from Agilent Technologies. Analysis was performed as described earlier (Dudek *et al*., 2010; Dudek *et al*., 2011).

Luciferase reporter gene assays

For luciferase reporter gene assays 5×10^5 A549 cells were transfected with 1 μg pcDNA plasmids containing the indicated NS1 genes (pcDNA3-NS1-T49, pcDNA3-NS1-T49A or pcDNA3-NS1-T49E) along with 0.5 μg luciferase reporter gene plasmids harbouring either the complete IFN promoter (pTATA-luc-IFN-β) or the IRF-3 domain only (pTATA-luc-4xIRF-3) using Trans IT-LT1 transfection reagent (Mirus Bio) according to the manufacturer's protocol. Twenty-four hours later, cells were transfected with 0.5 μg total RNA isolated from PR8-infected A549 cells (viral RNA) or from uninfected cells as control (cellular RNA) for additional 6 h and luciferase activity in cell lysates was determined as described elsewhere (Hillesheim *et al*., 2014).

RNA pulldown analysis

To elucidate the ability of NS1 to bind RNA, a protocol published previously was adapted (Habjan *et al*., 2008). 1.2×10^6 A549 cells were transfected with 2 μg pcDNA3 plasmids containing wt NS1 (pcDNA3-NS1-T49) or NS1 with the indicated mutations (pcDNA3-NS1-T49A or pcDNA3-NS1-T49E) or were mock transfected using Trans IT-LT1 transfection reagent (Mirus Bio) according to the manufacturer's protocol. Twenty-four hours later, the cells were lysed in RIPA buffer and cell lysates subjected to immunoprecipitations using mouse anti-NS1 antibody (clone NS1-23-1, IMV Münster) and protein G agarose beads (Roche) for 4 h at 4°C. Subsequently, beads were washed three times with RIPA buffer and incubated with 1 μg vRNA for additional 2 h at 4°C followed by washing with RIPA buffer. RNA bound to immunocomplexes was extracted using RNeasy kit from Qiagen and the relative amount of viral NS1 mRNA was detected by qRT-PCR.

Co-immunoprecipitations

For analysis of NS1-RIG-I complex formation 1.2×10^6 HEK293 cells were transfected with 1.5 μg of the pCAGGS-Flag-RIG-I construct, expressing FLAG-tagged RIG-I, along with 1.5 μg of pcDNA3-NS1-T49, pcDNA3-NS1-T49A or pcDNA3-NS1-T49E using Trans IT-LT1 transfection reagent (Mirus Bio) according to the manufacturer's protocol. After 48 h, cells were trypsinized and cell suspension was subjected to crosslinking with 1 mM DSP (Dithiobis[succinimidyl propionate]) (Sigma) for 30 min at 4°C, followed by quenching with 100 mM glycine (Roth) for 15 min at 4°C. Finally, the cells were lysed with RIPA buffer and RIG-I was immunoprecipitated with mouse anti-FLAG M2 antibody (Sigma-Aldrich) coupled to protein G agarose beads (Roche) overnight at 4°C. Immunocomplexes were resolved by SDS-PAGE and the co-precipitated NS1 protein was detected by Western blotting using mouse anti-NS1 antibody (clone NS1-23-1, IMV Münster). Detection of FLAG-tagged RIG-I by mouse anti-FLAG M2 antibody served as control to ascertain the amount of precipitated proteins.

For analysis of NS1-TRIM25 interaction 1.2×10^6 HEK293 cells were infected with PR8/NS1-T49, PR8/NS1-T49A or PR8/NS1-T49E at a MOI of 1, 5 or 10, respectively, ensuring comparable NS1 expression levels. Eighteen hours post infection (h p.i.), infected cells were washed with PBS and lysed in NP40 buffer (50 mM HEPES [pH 7.4], 150 mM NaCl and 1 % (v/v) NP40) containing protease inhibitors. From this, lysates TRIM25 was immunoprecipitated with mouse anti-TRIM25 antibody (BD Biosciences) coupled to protein G agarose beads (Roche) overnight at 4°C. After three washing steps with NP40 buffer, TRIM25 and the co-precipitated NS1 were detected by Western blotting using mouse anti-TRIM25 antibody (BD Biosciences) or mouse anti-NS1 antibody (clone NS1-23-1, IMV Münster).

Infection of mice and determination of viral lung titers

To analyse viral replication, *in vivo* C57Bl/6 mice or C57Bl/6 *Ifnar1*$^{-/-}$ mice were infected intranasally with 10^3 PFU of PR8/NS1-T49 or PR8/NS1-T49E in 50 μL PBS and virus titers were quantified by standard plaque titration 3 days later in 10% (w/v) lung tissue homogenates.

In silico prediction of RNA binding scores

The RNA–protein interaction prediction tool was employed to predict the RNA binding scores for NS1-T49, NS1-T49A and NS1-T49E (Muppirala *et al*., 2011). RNA–protein interaction prediction exploits the amino acid composition of protein sequences and ribonucleotide composition of RNA sequences to predict the probability that a given pair (protein and RNA) will

interact. Two classifiers, the Random Forest and Support Vector Machine are used to predict the RNA sequence binding affinity with a given protein sequence. The tool utilizes 2 non-redundant benchmark datasets of RNA–protein interactions, RPI2241 and RPI369, extracted from PRIDB, a comprehensive database of RNA-protein complexes extracted from the Protein Data Bank (PDB). The RNA sequence used for predicting the comparative RNA-NS1 protein interaction scores was obtained from PDB ID 2ZKO (Cheng *et al*., 2009).

Structural simulation of RNA binding by non-structural protein 1

The effect of the T49E substitution in NS1 on protein structure was calculated using the DUET server (Pires *et al*., 2014b). DUET uses an integrated computational approach (Site Directed Mutator and mutation Cutoff Scanning Matrix) for predicting effects of mutations on protein stability. Site Directed Mutator compares amino acid propensities for the wt and mutated proteins in the folded and unfolded states in order to estimate the free energy differences. Mutant Cutoff Scanning Matrix uses a machine learning method to predict the effects of missense mutations based on structural signatures (Topham *et al*., 1997; Pires *et al*., 2014a). Structural simulation was performed on PDB ID 2ZKO. The molecular graphic simulation was performed using Bioblender (Andrei *et al*., 2012).

Funding Information

This work was supported by Grant No. Lud2/017/13 from the Interdisciplinary Center of Clinical Research (IZKF), the Muenster Graduate School of Evolution (MGSE) and the DFG Collaborative Research Center SFB1009, University of Muenster, Germany. The Institute of Molecular Virology is part of the *FluResearchNet*, a nationwide research network on zoonotic influenza.

Acknowledgements

We are greatly thankful to Mirita Franz-Wachtel, Karsten Krug and Boris Macek from Proteome Center of the University of Tuebingen, Germany for phosphoproteomic analysis of the NS1 protein.

References

Andrei, R.M., Callieri, M., Zini, M.F., Loni, T., Maraziti, G., Pan, M.C., and Zoppè, M. (2012) Intuitive representation of surface properties of biomolecules using BioBlender. *BMC Bioinformatics* **13**(Suppl 4): S16.

Carpy, A., Krug, K., Graf, S., Koch, A., Popic, S., Hauf, S., and Macek, B. (2014) Absolute proteome and phosphoproteome dynamics during the cell cycle of Schizosaccharomyces pombe (Fission Yeast). *Mol Cell Proteomics* **13**: 1925–1936.

Cheng, A., Wong, S.M., and Yuan, Y.A. (2009) Structural basis for dsRNA recognition by NS1 protein of influenza A virus. *Cell Res* **19**: 187–195.

Dudek, S.E., Luig, C., Pauli, E.-K., Schubert, U., and Ludwig, S. (2010) The clinically approved proteasome inhibitor PS-341 efficiently blocks influenza A virus and vesicular stomatitis virus propagation by establishing an antiviral state. *J Virol* **84**: 9439–51.

Dudek, S.E., Wixler, L., Nordhoff, C., Nordmann, A., Anhlan, D., Wixler, V., and Ludwig, S. (2011) The influenza virus PB1-F2 protein has interferon antagonistic activity. *Biol Chem* **392**: 1135–44.

Gack, M.U., Albrecht, R.A., Urano, T., Inn, K.-S., Huang, I.-C., Carnero, E., *et al.* (2009) Influenza A virus NS1 targets the ubiquitin ligase TRIM25 to evade recognition by the host viral RNA sensor RIG-I. *Cell Host Microbe* **5**: 439–449.

García-Sastre, A. (2011) Induction and evasion of type I interferon responses by influenza viruses. *Virus Res* **162**: 12–18.

García-Sastre, A., Egorov, A., Matassov, D., Brandt, S., Levy, D.E., Durbin, J.E., *et al.* (1998) Influenza A virus lacking the NS1 gene replicates in interferon-deficient systems. *Virology* **252**: 324–330.

Habjan, M., Andersson, I., Klingström, J., Schümann, M., Martin, A., Zimmermann, P., *et al.* (2008) Processing of genome 5' termini as a strategy of negative-strand RNA viruses to avoid RIG-I-dependent interferon induction. *PLoS One* **3**: e2032.

Hale, B.G., Randall, R.E., Ortín, J., and Jackson, D. (2008) The multifunctional NS1 protein of influenza A viruses. *J Gen Virol* **89**: 2359–2376.

Hale, B.G., Knebel, A., Botting, C.H., Galloway, C.S., Precious, B.L., Jackson, D., *et al.* (2009) CDK/ERK-mediated phosphorylation of the human influenza A virus NS1 protein at threonine-215. *Virology* **383**: 6–11.

Hatada, E., and Fukuda, R. (1992) Binding of influenza A virus NS1 protein to dsRNA in vitro. *J Gen Virol* **73**(Pt 12): 3325–3329.

Hatada, E., Saito, S., Okishio, N., and Fukuda, R. (1997) Binding of the influenza virus NS1 protein to model genome RNAs. *J Gen Virol* **78**(Pt 5): 1059–1063.

Hillesheim, A., Nordhoff, C., Boergeling, Y., Ludwig, S., and Wixler, V. (2014) β-catenin promotes the type I IFN synthesis and the IFN-dependent signaling response but is suppressed by influenza A virus-induced RIG-I/NF-κB signaling. *Cell Commun Signal* **12**: 29.

Hoffmann, E., Neumann, G., Kawaoka, Y., Hobom, G., and Webster, R.G. (2000) A DNA transfection system for generation of influenza A virus from eight plasmids. *Proc Natl Acad Sci U S A* **97**: 6108–6113.

Hsiang, T.-Y., Zhou, L., and Krug, R.M. (2012) Roles of the phosphorylation of specific serines and threonines in the NS1 protein of human influenza A viruses. *J Virol* **86**: 10370–10376.

Hutchinson, E.C., Denham, E.M., Thomas, B., Trudgian, D.C., Hester, S.S., Ridlova, G., *et al.* (2012) Mapping the phosphoproteome of influenza A and B viruses by mass spectrometry. *PLoS Pathog* **8**: e1002993.

Krug, R.M. (2015) Functions of the influenza A virus NS1 protein in antiviral defense. *Curr Opin Virol* **12**: 1–6.

Macek, B., Mann, M., and Olsen, J.V. (2009) Global and site-specific quantitative phosphoproteomics: principles and applications. *Annu Rev Pharmacol Toxicol* **49**: 199–221.

Marc, D. (2014) Influenza virus non-structural protein NS1: interferon antagonism and beyond. *J Gen Virol* **95**: 2594–2611.

Mibayashi, M., Martínez-Sobrido, L., Loo, Y.-M., Cárdenas, W.B., Gale, M., and García-Sastre, A. (2007) Inhibition of retinoic

acid-inducible gene I-mediated induction of beta interferon by the NS1 protein of influenza A virus. *J Virol* **81**: 514–524.
Muppirala, U.K., Honavar, V.G., and Dobbs, D. (2011) Predicting RNA-protein interactions using only sequence information. *BMC Bioinformatics* **12**: 489.
Opitz, B., Rejaibi, A., Dauber, B., Eckhard, J., Vinzing, M., Schmeck, B., *et al.* (2007) IFNbeta induction by influenza A virus is mediated by RIG-I which is regulated by the viral NS1 protein. *Cell Microbiol* **9**: 930–938.
Pires, D.E.V., Ascher, D.B., and Blundell, T.L. (2014a) mCSM: predicting the effects of mutations in proteins using graph-based signatures. *Bioinformatics* **30**: 335–42.
Pires, D.E.V., Ascher, D.B., and Blundell, T.L. (2014b) DUET: a server for predicting effects of mutations on protein stability using an integrated computational approach. *Nucleic Acids Res* **42**: W314–9.
Qian, X.Y., Chien, C.Y., Lu, Y., Montelione, G.T., and Krug, R. M. (1995) An amino-terminal polypeptide fragment of the influenza virus NS1 protein possesses specific RNA-binding activity and largely helical backbone structure. *RNA* **1**: 948–956.
Qiu, Y., and Krug, R.M. (1994) The influenza virus NS1 protein is a poly(A)-binding protein that inhibits nuclear export of mRNAs containing poly(A). *J Virol* **68**: 2425–2432.
Rajsbaum, R., Albrecht, R.A., Wang, M.K., Maharaj, N.P., Versteeg, G.A., Nistal-Villán, E., *et al.* (2012) Species-specific inhibition of RIG-I ubiquitination and IFN induction by the influenza A virus NS1 protein. *PLoS Pathog* **8**: e1003059.
Topham, C.M., Srinivasan, N., and Blundell, T.L. (1997) Prediction of the stability of protein mutants based on structural environment-dependent amino acid substitution and propensity tables. *Protein Eng* **10**: 7–21.
Venselaar, H., te Beek, T.A., Kuipers, R.K., Hekkelman, M.L., and Vriend, G. (2010) Protein structure analysis of mutations causing inheritable diseases. An e-Science approach with life scientist friendly interfaces. *BMC Bioinformatics* **11**: 548.

Supporting information

Additional supporting information may be found in the online version at the publisher's web site:

Fig. S1. Phosphorylation of NS1 at T49 but not T215 significantly attenuates viral replication in A549 cells. (A, B) Multi-cycle replication kinetics of recombinant PR8 viruses containing wt NS1 or NS1 with different mutations in A549 cells. Cells were infected with low multiplicity of infection (MOI = 0.01 (A) or MOI = 0.1 (B)) and supernatants of infected cells were analysed for virus progeny by standard plaque assay. Data represents mean ± SD of three (A) or two (B) independently repeated experiments. One-way ANOVA followed by Dunnett's multiple comparisons test using T49 or T215 as controls was used for statistical analysis of each time point separately (* $p \leq 0.05$, ** $p \leq 0.01$, *** $p \leq 0.001$, n.s. = not significant). For statistics of two independently repeated experiments each biological replicate was taken into account.